

Supplementary Materials for

# Analysis of Dynamic Recrystallization During the Reduction Pretreatment Process Using a Multiscale Model

Die Wu <sup>1,2</sup>, Zhen Ning <sup>1,2</sup>, Yanlin Zhu <sup>2</sup> and Wei Yu <sup>1,\*</sup>

- <sup>1</sup> National Engineering Research Center of Flat Rolling Equipment, University of Science and Technology Beijing, Beijing 100083; 17778606018@163.com (D.W.); zhenning410@163.com (Z.N.);  
<sup>2</sup> Institute for Mathematical and Computational Materials Science, Chengdu Advanced Metal Materials Industry Technology Research Institute Co., Ltd., Chengdu 610300, Sichuan, China; 17778606018@163.com (D.W.); zhenning410@163.com (Z.N.); ali.yanlinzhu@outlook.com (Y.Z.)  
 \* Correspondence: yuwei@nercar.ustb.edu.cn; Tel.: +86-13001183873

## Section S1 Material and thermal compression experiments

The material used in the study was 42CrMo steel, and its chemical composition is shown in Table S1. It was machined into a  $\Phi 10 \times 15$  mm specimen and a single-pass hot compression experiment was performed on a Gleeble 3800 thermal simulation experiment machine.

**Table S1.** Chemical composition of experimental steel.

C	Si	Mn	Cr	Mo	Ni	Cu	P	S	Fe
0.39	0.24	0.72	1.12	0.189	0.09	0.01	0.012	0.004	bal

The hot compression process is designed with deformation temperatures of 1223, 1273, 1323, 1373 and 1473 K and strain rates of 0.001, 0.005, 0.01, 0.05 and 0.1 s<sup>-1</sup>. The data for deformation temperatures of 1273, 1373 and 1473 K and strain rates of 0.001, 0.01 and 0.1 s<sup>-1</sup> were used for modelling, while the other data were used for model validation. The thermal compression process is shown in Figure S1: (1) the specimen was heated to 1473 K at 10 K/s; (2) it was held for 5 min to ensure tissue homogeneity; (3) it was then cooled to the deformation temperature at a cooling rate of 10 K/s; (4) for 20 s to ensure temperature uniformity; (5) then a single-pass hot compression experiment was performed at strain rates of 0.001, 0.01 and 0.1 s<sup>-1</sup>, respectively, with a maximum true strain; (6) after compression was complete, rapid cooling to room temperature was performed.

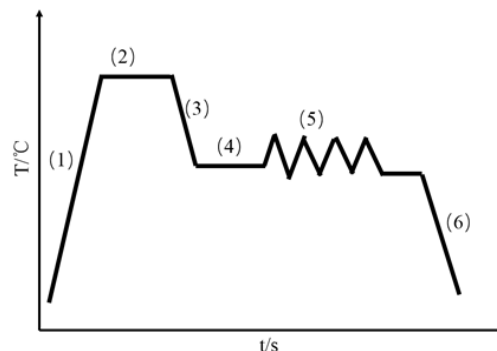


**Figure S1.** Thermal compression process route.

In this study, the material parameters used for MPFM are required to be obtained from the thermocompression stress-strain curves. Figure S2 shows the stress-strain curve of 42CrMo steel under different process parameters.

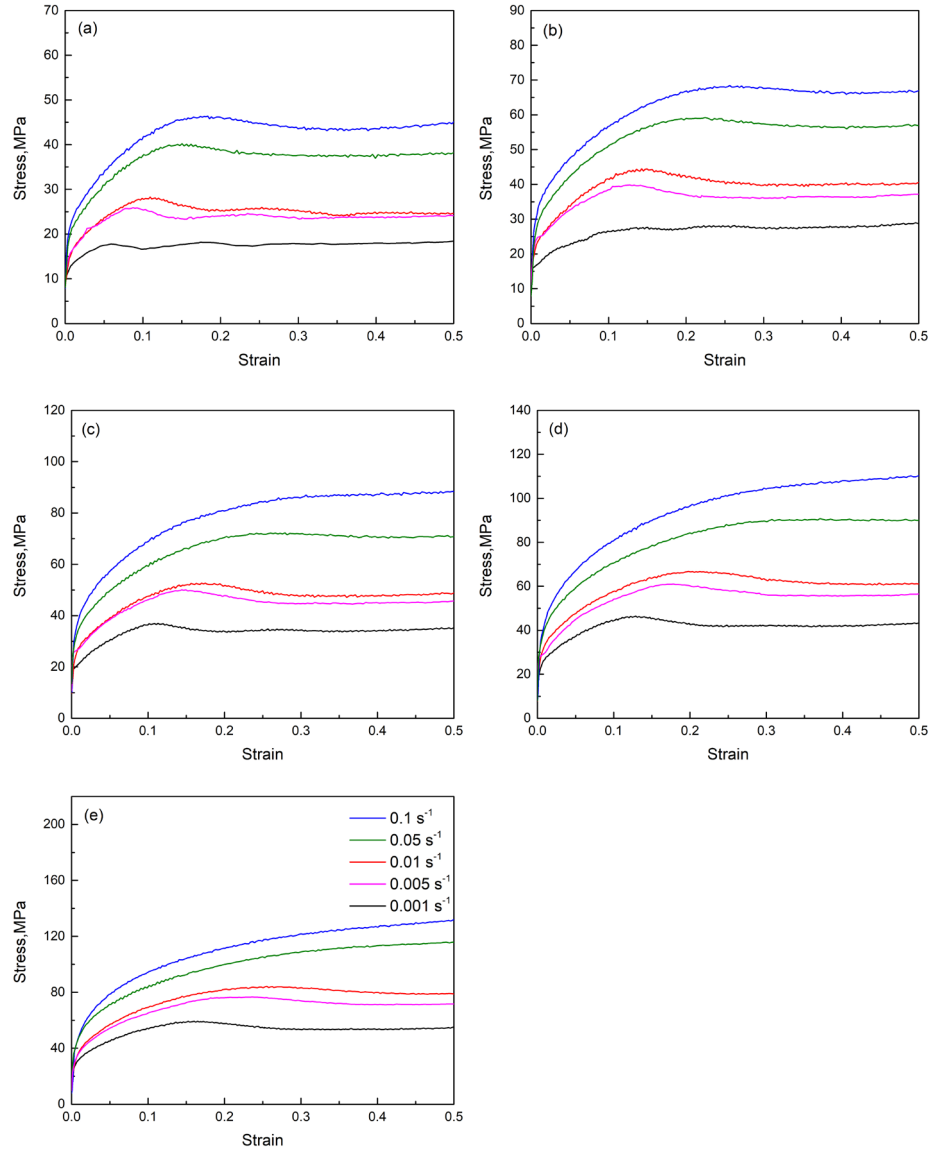


**Figure S2.** Stress-strain curves at different temperatures: (a) 1473 K; (b) 1373 K; (c) 1323 K; (d) 1273 K; (e) 1223 K.

### Section S2 Characteristic stress of experimental steel

To construct a dynamic recrystallization model for low-alloy steel, it is essential to obtain the characteristic stresses during the metal's hot deformation process: initial stress ( $\sigma_0$ ), critical stress for dynamic recrystallization ( $\sigma_c$ ), peak stress ( $\sigma_p$ ), saturated stress during hot working ( $\sigma_s$ ), and steady-state stress for dynamic recrystallization ( $\sigma_{ss}$ ). The relationship between these stresses and the Zener-Hollomon parameter,  $Z$ , must also be established. To eliminate irregularities and fluctuations in the flow stress curves obtained from hot compression tests, a 7th-order polynomial fitting was applied to the experimental curves using Matlab software, as shown in Figure S3(a).

To obtain the characteristic stresses during the material's hot deformation process, a relationship between the work hardening rate ( $\theta$ ) and stress ( $\sigma$ ) was constructed, as shown in Figure S3(b). According to previous studies [1], the critical stress for dynamic recrystallization corresponds to the point where the second derivative of the work hardening rate with respect to stress equals zero, that is, when  $d^2\theta/d\sigma^2=0$ . The saturated stress is obtained by drawing a tangent to the  $\theta$ - $\sigma$  curve at the point where  $d\theta/d\sigma=0$ . The peak stress and steady-state stress are the stress values where the first and second derivatives of the  $\theta$ - $\sigma$  curve equal zero, respectively.

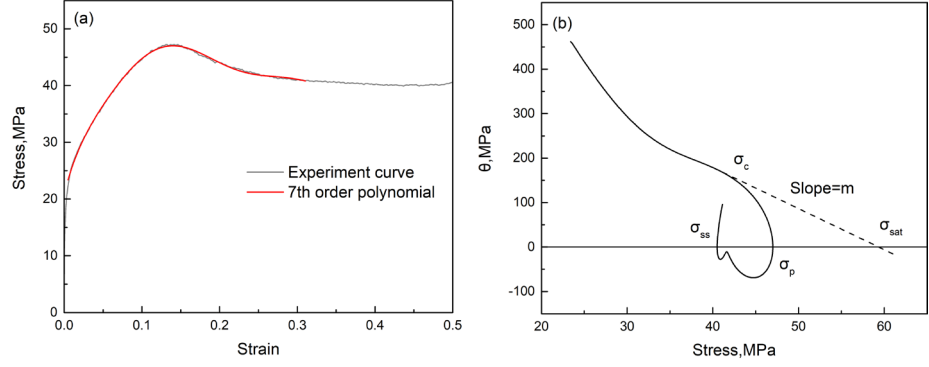


**Figure S3.** Diagram of Characteristic Stress Acquisition: (a) 7th-order Polynomial Fitting of Flow Stress Curve; (b) Stress-Work Hardening Rate Curve.

The relationship between  $\sigma_p$  and  $Z$  can be expressed as:

$$\sigma_p = AZ^n \quad (S1)$$

where  $A$  and  $n$  are the fitted parameters.

The relationship between  $Z$  and the strain rate and deformation temperature is:

$$Z = \dot{\varepsilon} \exp\left(\frac{Q_{act}}{RT}\right) \quad (S2)$$

where  $\dot{\varepsilon}$  is the strain rate,  $Q_{act}$  is the deformation activation energy,  $R$  is the standard gas constant,  $T$  is the deformation temperature.

From Equations S1 and S2, it follows that:

$$\sigma_p = A \left( \dot{\varepsilon} \exp\left(\frac{Q_{act}}{RT}\right) \right)^n \quad (S3)$$

$$\ln(\sigma_p) = \ln(A) + n \left( \ln(\dot{\varepsilon}) + \frac{Q_{act}}{RT} \right) \quad (S4)$$

The peak stress and strain rate at different deformation temperatures are brought into Equation S4, and the average value is calculated by calculating the slope of the curve. The average value of  $n$  and  $Q_{act}$  is calculated using the above method, as shown in Figure S4.

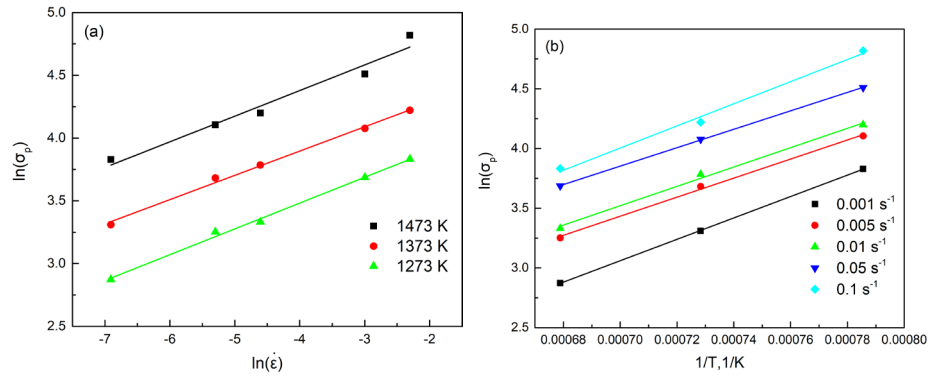


**Figure S4.** Calculation process for parameter  $n$  and activation energy of deformation  $Q_{act}$ .

The final relationship between peak stress and  $Z$  is:

$$\sigma_p = 0.31(Z)^{0.1822} = 0.31\left(\dot{\varepsilon} \exp\left(\frac{362000}{RT}\right)\right)^{0.1822} \quad (S5)$$

The relationship between peak stress and other characteristic stresses is shown in Figure S5.

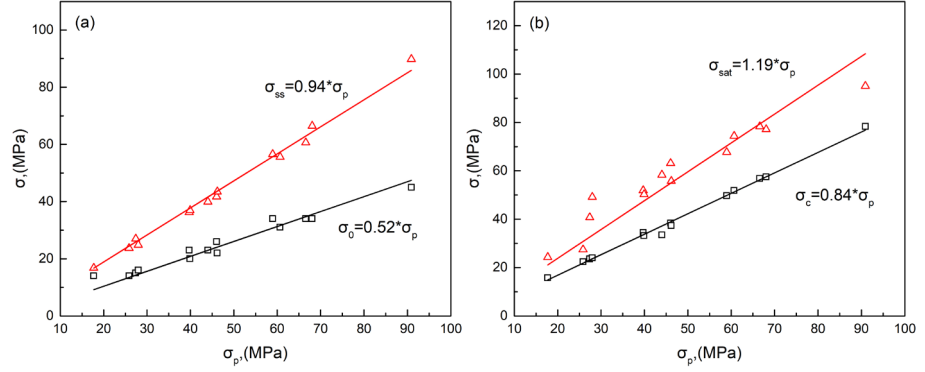


**Figure S5.** Relationship between peak stress and other characteristic stresses: (a) initial stress and steady-state stress; (b) critical stress and saturation stress.

As can be seen in the Figure S5, there is a linear relationship between the peak stress and the other characteristic stresses. The relationship between the peak stress and other characteristic stresses obtained by fitting is:

$$\sigma_0 = 0.52 \sigma_p \quad (S6)$$

$$\sigma_{ss} = 0.94 \sigma_p \quad (S7)$$

$$\sigma_c = 0.84 \sigma_p \quad (S8)$$

$$\sigma_{sat} = 1.19 \sigma_p \quad (S9)$$

### Section S3 Dislocation evolution model

During thermal deformation, the dislocation density is controlled by two processes: work hardening and dynamic recovery. In this study, the KM model established by Kocks and Mecking [2-4] was used to describe these two processes. The evolution of the dislocation density within the grain during thermal deformation can be expressed as:

$$\frac{d\rho}{d\varepsilon} = k_1 \sqrt{\rho} - k_2 \rho \quad (S10)$$

where  $k_1$  is a constant related to work hardening,  $k_2$  is the softening parameter associated with the dynamic recovery.

Integrating Equation S10 gives:

$$\sqrt{\rho} = \sqrt{\rho_s} + (\sqrt{\rho_0} - \sqrt{\rho_s}) \exp\left(\frac{k_2}{2} \varepsilon\right) \quad (S11)$$

where  $\rho_s$  is the dislocation density of the matrix at saturation stress,  $\rho_0$  is the dislocation density of the matrix at the initial stress. According to the relationship between dislocation density and stress:

$$\sigma = \alpha \mu b \sqrt{\rho} \quad (\text{S12})$$

it can be obtained that:

$$\sigma = \sigma_s + (\sigma_0 - \sigma_s) \exp\left(\frac{k_2}{2} \varepsilon\right) \quad (\text{S13})$$

Differentiating both sides of Equation S13 with respect to the variable yields:

$$\frac{d\sigma}{d\varepsilon} = \frac{k_2}{2} \sigma - \frac{k_2}{2} \sigma_s \quad (\text{S14})$$

From equation S14, it can be seen that the value of  $k_2$  is related to the slope of the work hardening rate-stress curve,  $m$ , as shown in Figure S2(b),  $k_2 = 2m$ , and the value of  $m$  can be obtained from the work hardening rate-stress curve. It is also known that at the saturation stress, the increment of dislocation density with strain is 0:

$$k_1 \sqrt{\rho_s} - k_2 \rho_s = 0 \quad (\text{S15})$$

The relationship between  $k_1$  and  $k_2$  is:

$$k_1 = k_2 \sqrt{\rho_s} \quad (\text{S16})$$

#### Section S4 Nucleation rate

Studies have shown that the nucleation rate of dynamic recrystallisation is related to the strain rate and deformation temperature. Therefore, the nucleation rate calculation formula used in this study is [5, 6]:

$$n_{DRX} = C \dot{\varepsilon}^m \exp\left(-\frac{Q_a}{RT}\right) \quad (\text{S17})$$

where  $C$  is the fitting constant,  $m$  is a constant related to the strain rate, and  $Q_a$  is the nucleation activation energy.

The volume fraction of dynamic recrystallisation can be obtained from the nucleation rate and average size of dynamic recrystallisation:

$$X_{\text{drx,exp}} = n t \frac{4}{3} \pi r_d^3 \quad (\text{S18})$$

where  $t$  is time,  $r_d$  is the average size of the recrystallized grains.

The volume fraction of recrystallisation and the average grain size can be obtained from the stress-strain curve and Equations S18 and S19:

$$X_{\text{drx,exp}} = \frac{\sigma_{\text{drv}} - \sigma_{\text{exp}}}{\sigma_{\text{sat}} - \sigma_{\text{ss}}} \quad (\text{S19})$$

where  $\sigma_{\text{drv}}$  is the stress during the thermal deformation process when only work hardening and dynamic recovery occur, which can be obtained by substituting the work hardening index obtained above into Equations S13;  $\sigma_{\text{exp}}$  is the stress obtained from the experiment.

The schematic diagram for calculating the volume fraction of dynamic recrystallisation is shown in Figure S6.

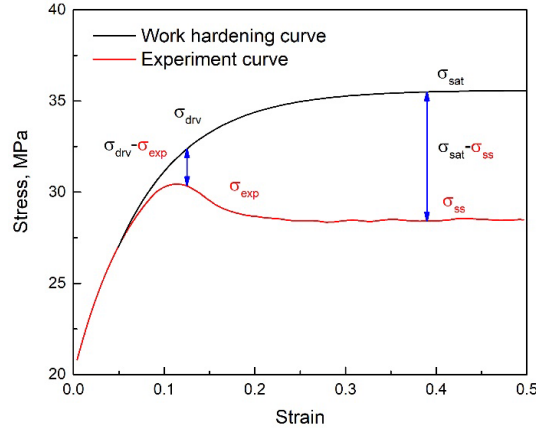


**Figure S6.** Schematic diagram for calculating the volume fraction of dynamic recrystallisation.

The relationship between the average dynamic recrystallisation grain size and stress is shown below [7, 8]:

$$\frac{\sigma_{ss}}{\mu} \left( \frac{2r_d}{b} \right)^n = K \quad (\text{S20})$$

In this formula, the value of the index  $n$  is  $2/3$ , and  $K$  is a constant with a value of 10.

Using Equations S18 and S19 and the experimentally obtained stress-strain curves, the curve of the nucleation rate as a function of deformation temperature and strain rate can be obtained, as shown in Figure S7. By curve fitting, the parameters in equation S17 can be obtained.

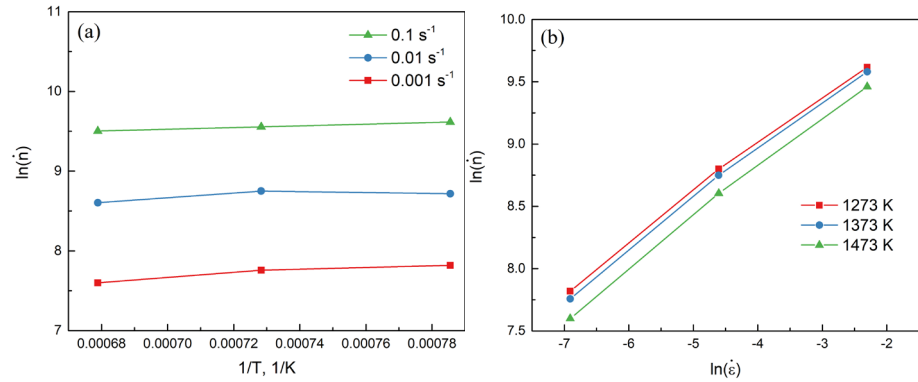


**Figure S7.** Variation of nucleation rate with temperature and strain rate: (a) temperature; (b) strain rate.

### Section S5 Statistical methods for the results of multi-phase field simulations

During the dynamic recrystallisation simulation, the stress, average grain size, and dynamic recrystallisation volume fraction at each time step need to be calculated. The stress can be calculated using Equation S12, while the average grain size,  $\bar{d}$ , and dynamic recrystallisation volume fraction,  $X_{\text{drx,cal}}$ , are calculated using the following equations:

$$\bar{d} = 2 \sqrt{\frac{S_{\text{Total}}}{N\pi}} \quad (\text{S21})$$

$$X_{\text{drx,cal}} = \frac{\sigma_{\text{drv}} - \sigma_{\text{cal}}}{\sigma_{\text{sat}} - \sigma_{\text{ss}}} \quad (\text{S22})$$

---

where  $S_{\text{Total}}$  is the total area of the simulation domain,  $N$  is the total number of grains in the simulation domain at the current time step,  $\sigma_{\text{cal}}$  is the stress calculated by the phase field model.

## References

1. Jonas J J, Queleuennec X, Jiang L, et al. The Avrami kinetics of dynamic recrystallization[J]. *Acta Materialia*, 2009,57(9):2748-2756.
2. Kocks U F. Laws for Work-Hardening and Low-Temperature Creep[J]. *J.eng.mater.tech*, 1976,98(1):76-85.
3. Mecking H. A Mechanism for Static and Dynamic Recovery[J]. 1979:345-350.
4. Mecking H, Kocks U F. Kinetics of Flow and Strain-Hardening[J]. *Acta Metallurgica*, 1981,29(11):1865-1875.
5. Peczak P, Luton M J. The effect of nucleation models on dynamic recrystallization II. Heterogeneous stored-energy distribution[J]. *Philosophical Magazine B Physics of Condensed Matter*, 1993,68(1):115-144.
6. Huang K, Logé R E. A review of dynamic recrystallization phenomena in metallic materials[J]. *Materials & Design*, 2016,111:548-574.
7. Derby B. The dependence of grain size on stress during dynamic recrystallisation[J]. *Acta Metallurgica et Materialia*, 1991,39(5):955-962.
8. Derby, B. Dynamic recrystallisation: The steady state grain size[J]. *Scripta Metallurgica et Materialia*, 1992,27(11):1581-1585.